

Coupled finite element/boundary element method for semiconductor quantum devices with exposed surfaces

Minhan Chen and Wolfgang Porod

Department of Electrical Engineering, University of Notre Dame, Notre Dame, Indiana 46556

David J. Kirkner

Department of Civil Engineering and Geological Sciences, University of Notre Dame, Notre Dame, Indiana 46556

(Received 21 June 1993; accepted for publication 11 November 1993)

We present a study of the boundary conditions for the potential at exposed semiconductor surfaces in split-gate structures, which views the exposed surface as the interface between the semiconductor and air. A two-dimensional numerical algorithm is presented for the coupling between the nonlinear Poisson equation in the semiconductor (finite element method) and Laplace's equation in the dielectric (boundary element method). The utility of the coupling method is demonstrated by simulating the potential distribution in an *n*-type AlGaAs/GaAs split-gate quantum wire structure within a semiclassical Thomas-Fermi charge model. We also present a comparison of our technique to more conventional Dirichlet and Neumann boundary conditions.

I. INTRODUCTION

Recent advances in nanostructure fabrication have made it possible to realize semiconductor quantum devices by further confining a two-dimensional layer of electrons into wires or dots in which quantum effects are significant.^{1,2} Typically, such device structures are defined by metallic split gates as schematically depicted in Fig. 1. In order to understand the potential distribution in these structures, one has to solve the Poisson equation in the two-dimensional problem domain,

$$\epsilon \nabla^2 \phi = -\rho. \quad (1)$$

Here, ϕ is the confining electrostatic potential, ϵ is the dielectric constant of the respective material, and ρ is the charge density, which may depend upon the potential and for which different charge models have been developed.³ Since Eq. (1) is a boundary value problem, one needs to know the values of the potentials and/or fluxes at the various boundaries. In particular at the exposed semiconductor surface, it has proven difficult to formulate appropriate boundary conditions. This is a crucial problem, especially in nanostructures where the charge carriers reside close to the surface, and a different choice for the boundary condition at the exposed surface may result in a noticeable difference in the confining potential of the quantum device. Highly accurate models of the potential variation will be needed to realize recently proposed computing architectures for quantum devices, so-called quantum cellular automata, which consist of cells of coupled quantum dots which are occupied by only a few electrons.⁴

In recent numerical studies,⁵⁻¹¹ the potential variation in structures like the one shown in Fig. 1 has been treated as a boundary value problem on the semiconductor domain and various boundary conditions have been assumed on the exposed semiconductor surface. One common approach is to utilize a Dirichlet boundary condition which

simulates surface Fermi-level pinning at a characteristic energy level in the band gap,⁹⁻¹¹

$$\phi|_s = -\phi_{\text{pin}}. \quad (2)$$

This approximation leads to an unrealistic discontinuous step in the potential energy at the edge of the biased gate between the values of the applied gate potential and the Fermi-level pinning. Another commonly used approach is to employ a Neumann boundary condition where one assumes a certain value for the outward normal electric field on the exposed semiconductor surface,^{5,6}

$$\epsilon_s \frac{\partial \phi}{\partial \mathbf{n}} \Big|_s = Q_{\text{int}}. \quad (3)$$

\mathbf{n} is the outward normal unit vector of the boundary, ϵ_s is the dielectric constant of the semiconductor, and Q_{int} is the charge density on the exposed surface. It can be shown that this approximation is only valid if the exposed semiconductor surface is large and smooth.¹² In typical split-gate structures used for quantum devices, the confined electron gas is very close to the exposed semiconductor surface and the separation between the split gates is rather small. The validity of the above two boundary conditions, thus, appears doubtful.

In this paper, we adopt an alternative viewpoint and develop an algorithm for its implementation: We view as the natural problem domain the semiconductor *and* the dielectric, as schematically shown in Fig. 2. Thus the artificial boundary conditions at the exposed semiconductor surface are replaced by more physical matching conditions at the interface between the semiconductor and dielectric. We assume that the potential ϕ is continuous across this interface and that the jump in the normal electric flux density is equal to the interface charge density,

$$\phi|_s = \phi|_d, \quad (4)$$

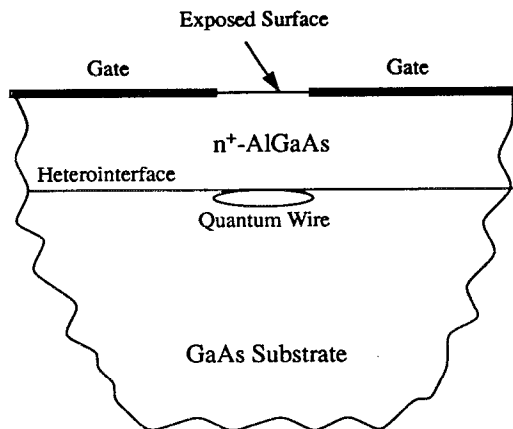


FIG. 1. Typical problem domain for quantum devices defined by metallic gates. Shown are the multilayer semiconductor regions and the exposed surface between the gates.

$$\epsilon_s \frac{\partial \phi}{\partial \mathbf{n}} \Big|_s - \epsilon_d \frac{\partial \phi}{\partial \mathbf{n}} \Big|_d = Q_{\text{int}}, \quad (5)$$

where $\phi|_s$ is the potential on the semiconductor side of the interface and $\phi|_d$ is the one on the dielectric side, and Q_{int} is the surface charge density at the semiconductor/dielectric interface.

Several numerical methods may be employed to solve the above problem on the enlarged domain. Applying the finite element method or the finite difference method to both the dielectric and semiconductor regions would be the most direct approach. However, direct discretization of both domains would significantly increase the size of the system of equations compared to the original problem, re-

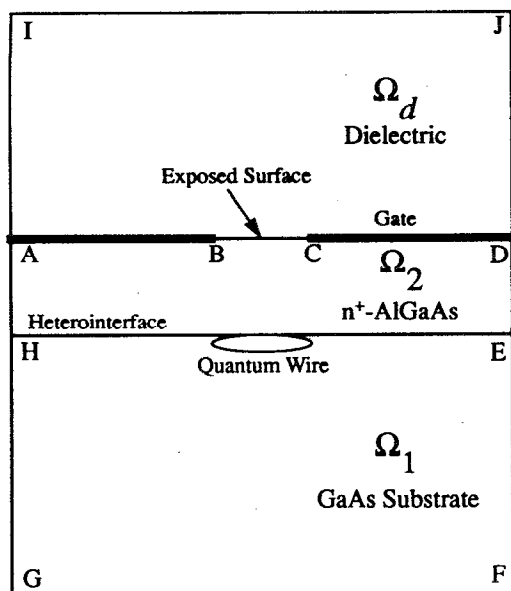


FIG. 2. The full problem domain consisting of both the semiconductor (regions Ω_1 and Ω_2) and the dielectric (region Ω_d). The exposed semiconductor surface is treated as the interface between the semiconductor and the dielectric.

sulting in an increase in memory requirements and operation counts. Also, since the dielectric domain extends to infinity, it would be difficult to discretize by conventional numerical techniques. To overcome these disadvantages, we develop a new algorithm which couples a finite element solution¹³ of Poisson's equation in the semiconductor to a boundary element solution¹⁴ of Laplace's equation in the dielectric. This coupling algorithm between the finite element method (FEM) and the boundary element method (BEM) is referred to as FBEM.

The main virtue of our problem formulation and the FBEM algorithm consists in providing an accurate solution of the potential in the dielectric domain, yet the system of equations to be solved is not significantly larger than the one for the semiconductor domain alone. Because of the inherently more complex material system, the potential in the semiconductor domain is obtained by employing a finite element discretization of the entire semiconductor region. Since the dielectric domain is homogeneous and charge free, Poisson's equation there reduces to Laplace's equation, for which we know the fundamental solution, that is, the Green's function for the infinite domain. By employing a boundary integration with this known Green's function, one can obtain both the potential *and* the electric field along the boundary of the dielectric if one only knows either the potential *or* the electric field on the boundary of the dielectric domain. Furthermore, the potential and the electric field within the whole dielectric domain then can be easily calculated by using the Green's function with the completed boundary values of potential and electric field. In the boundary element method,¹⁴ since only the boundary needs to be discretized, the size of the resultant system of equations is much smaller compared to the one generated by other numerical techniques. After employing the finite element formulation in the semiconductor domain and the boundary element formulation in the dielectric domain, we obtain two systems of equations which represent the discretized forms of the original equations. Coupling of the finite element system of equations to the boundary element system of equations is accomplished by transforming the boundary element system of equations to an equivalent finite element system of equations. Similar coupling techniques have also been successfully applied in elastostatics in civil engineering.¹⁵ Assembling this equivalent system of equations into the native finite element system of equations along the interface between the semiconductor and dielectric, implements the matching conditions on the exposed semiconductor surface.

The remainder of this paper is organized as follows. In Sec. II, we present the precise formulation of the problem including the boundary conditions. We also outline the numerical formulation of our FBEM solution algorithm, with the mathematical details deferred to the appendix. In Sec. III, we present example results of the FBEM calculation for an *n*-type AlGaAs/GaAs quantum wire structure under bias conditions, and we compare these to the ones obtained with the usual Dirichlet and Neumann boundary conditions. Concluding remarks are given in Sec. IV. Appendix A contains the details of the finite element formu-

lation in the semiconductor domain, and Appendix B of the boundary element formulation in the dielectric. Appendix C explains the procedure for coupling these two regions into one global system of equations.

II. FORMULATION OF THE PROBLEM

A. Problem statement

We solve the two-dimensional potential problem in the domain shown in Fig. 2, where region Ω_1 with boundary $\partial\Omega_1$ and Ω_2 with boundary $\partial\Omega_2$ are semiconductor domains in which the nonlinear Poisson equation governs, and region Ω_d with boundary $\partial\Omega_d$ is the dielectric domain in which Laplace's equation governs. We are mostly interested in the variation of the conduction band edge in the semiconductor, which depends upon the local potential in the form $E_C(\phi) = E_C^b - e\phi$, where E_C^b is the conduction band edge in the bulk which is determined by the background doping density. Below, we state the problem in terms of the reduced variable $u = [E_C(\phi) - E_F]/kT$ which measures the separation between the conduction band edge and the Fermi level E_F in units of the thermal energy kT .

In order to perform a device simulation, an artificial boundary is introduced, and the problem domain is defined by the polygonal region shown in Fig. 2. We assume that the artificial boundaries *I-A-H-G-F-E-D-J-I* are sufficiently far removed from the exposed surface and the heterointerface region that a zero normal gradient boundary condition, $\partial u/\partial \mathbf{n} = 0$, may be used. In Fig. 2, the boundaries *B-A* and *D-C* are Schottky contacts where the potential is known. The boundary *C-B* is the exposed semiconductor surface. Mathematically *C-B* is the interface between the region Ω_2 and the region Ω_d . Across this interface, the potential is continuous and the jump in the normal electric flux density is equal to the interface charge density. For the heterointerface *E-H*, between the semiconductors, a linear constraint, $u_1 - u_2 = \Delta u$, is employed. Here boundaries are labeled in a counterclockwise direction and the normal direction of the boundary has the relation $\mathbf{n}_{MN} = -\mathbf{n}_{NM}$.

The problem to be solved can be posed as follows:

P1. Find:

$$u_1, u_2, u_d, \quad (6)$$

such that

$$\epsilon_l \nabla^2 u_l(x, y) = -f[u_l(x, y)], \quad (x, y) \in \Omega_l, \quad l = 1, 2, \quad (7)$$

$$\epsilon_d \nabla^2 u_d(x, y) = 0, \quad (x, y) \in \Omega_d, \quad (8)$$

with boundary conditions:

$$u_2 = u_d = u_{g1}, \quad \text{on } \partial\Omega_{BA}, \quad (9)$$

$$u_2 = u_d = u_{g2}, \quad \text{on } \partial\Omega_{DC}, \quad (10)$$

$$\frac{\partial u_1}{\partial \mathbf{n}} = 0, \quad \text{on } \partial\Omega_{HG}, \partial\Omega_{FE}, \partial\Omega_{GF}, \quad (11)$$

$$\frac{\partial u_2}{\partial \mathbf{n}} = 0, \quad \text{on } \partial\Omega_{AH}, \partial\Omega_{ED}, \quad (12)$$

$$\frac{\partial u_d}{\partial \mathbf{n}} = 0, \quad \text{on } \partial\Omega_{IA}, \partial\Omega_{DJ}, \partial\Omega_{JI}, \quad (13)$$

and with interface conditions:

$$u_2 - u_d = 0, \quad \text{on } \partial\Omega_{CB}, \quad (14)$$

$$\epsilon_2 \frac{\partial u_2}{\partial \mathbf{n}} - \epsilon_d \frac{\partial u_d}{\partial \mathbf{n}} = \frac{e}{kT} Q_{\text{int}}, \quad \text{on } \partial\Omega_{CB}, \quad (15)$$

$$u_1 - u_2 = \Delta u, \quad \text{on } \partial\Omega_{EH}, \quad (16)$$

$$\epsilon_1 \frac{\partial u_1}{\partial \mathbf{n}} - \epsilon_2 \frac{\partial u_2}{\partial \mathbf{n}} = 0, \quad \text{on } \partial\Omega_{EH}, \quad (17)$$

where ϵ is the dielectric constant of the domain, and u_{g1} and u_{g2} represent the known values of the gate potential on the boundaries $\partial\Omega_{BA}$ and $\partial\Omega_{DC}$, respectively. Δu is the jump in the conduction band edge at the heterointerface $\partial\Omega_{EH}$, $f(u_l) \equiv f_l = e\rho_l/kT$, is the charge density term in the domain Ω_l , and Q_{int} is the interface charge density on the interface $\partial\Omega_{CB}$. In general, Q_{int} and ρ_l may be a function of the electrostatic potential, that is, $Q_{\text{int}} = Q_{\text{int}}(u)$ and $\rho_l = \rho_l(u)$.

B. Numerical formulation

The boundary value problem posed in Sec. II A recognizes explicitly the fact that the "open boundary," $\partial\Omega_{CB}$ is in fact an interface between the semiconductor and the dielectric. This obviates the need to assume a boundary condition on $\partial\Omega_{CB}$ as is often done. The potential on $\partial\Omega_{CB}$ and the electric flux across $\partial\Omega_{CB}$ are part of the solution. This boundary value problem may be solved by a number of different ways. Generally, detailed knowledge of the potential in the interior of the dielectric domain is not required, which suggests a boundary integral approach, whereas a finite element approach is more natural in the semiconductor domain. The main ideas of our approach employed herein are given below, and the mathematical details are explained in the appendix.

We recast the problem in the semiconductor domain as a weak variational problem suitable for application of the finite element method, as shown in Appendix A. In doing so, we proceed as if a flux boundary condition were specified on $\partial\Omega_{CB}$. The discretized form of Poisson's equation then yields the following linear system:

$$\begin{aligned} \mathbf{K}_{11} \mathbf{u}_0^s + \mathbf{K}_{12} \mathbf{u}_{BC}^s &= \mathbf{p}_f^s, \\ \mathbf{K}_{12}^T \mathbf{u}_0^s + \mathbf{K}_{22} \mathbf{u}_{BC}^s &= \mathbf{p}_{BC}^s. \end{aligned} \quad (18)$$

\mathbf{K} is the stiffness matrix, and \mathbf{u}_{BC}^s and \mathbf{p}_{BC}^s contain the potentials and nodal forces, respectively, at the nodes on the interface $\partial\Omega_{BC}$ between the semiconductor and the dielectric, whereas \mathbf{u}_0^s and \mathbf{p}_f^s contain the potential and nodal forces, respectively, at all other nodes in the semiconductor domain. The details of the FEM formulation in the semiconductor domain are given in Appendix A.

Since the fundamental solution of Laplace's equation (8) is known, a boundary integral technique can be employed for the dielectric domain, as detailed in Appendix B. Again, we proceed as if a flux boundary condition were

specified on $\partial\Omega_{CB}$. The discretized form of Laplace's equation then yields the following linear system:

$$\begin{aligned} \mathbf{S}_{11}\mathbf{u}_0^d + \mathbf{S}_{12}\mathbf{u}_{BC}^d &= \mathbf{p}_0^d, \\ \mathbf{S}_{21}\mathbf{u}_0^d + \mathbf{S}_{22}\mathbf{u}_{BC}^d &= \mathbf{p}_{BC}^d. \end{aligned} \quad (19)$$

\mathbf{S} is the equivalent stiffness matrix, and \mathbf{u}_{BC}^d and \mathbf{p}_{BC}^d contain the potentials and nodal forces, respectively, at the nodes on the interface $\partial\Omega_{BC}$ between the semiconductor and the dielectric, whereas \mathbf{u}_0^d and \mathbf{p}_0^d contain the potential and nodal forces, respectively, at all other nodes on the boundary of the dielectric domain. The details of the BEM formulation are given in Appendix B.

Both domains, semiconductor and dielectric, are coupled through the matching conditions at the exposed surface, (14) and (15). In discretized form, they read

$$\mathbf{u}_{BC}^s = \mathbf{u}_{BC}^d = \mathbf{u}_{BC}, \quad (20)$$

$$\mathbf{p}_{BC}^s + \mathbf{p}_{BC}^d = \mathbf{q}. \quad (21)$$

As described in Appendix C, the above matching conditions then couple these two problems, Eqs. (18) for the semiconductor and Eqs. (19) for the dielectric, to form a new global system of equations:

$$\begin{pmatrix} \mathbf{S}_{11} & \mathbf{S}_{12} & \mathbf{0} & \mathbf{0} \\ \mathbf{S}_{21} & \mathbf{S}_{22} & \mathbf{0} & \mathbf{I} \\ \mathbf{0} & \mathbf{K}_{12} & \mathbf{K}_{11} & \mathbf{0} \\ \mathbf{0} & \mathbf{K}_{22} & \mathbf{K}_{12}^T & -\mathbf{I} \end{pmatrix} \begin{pmatrix} \mathbf{u}_0^d \\ \mathbf{u}_{BC}^d \\ \mathbf{u}_0^s \\ \mathbf{p}_{BC}^s \end{pmatrix} = \begin{pmatrix} \mathbf{p}_0^d \\ \mathbf{q} \\ \mathbf{p}_f^s \\ \mathbf{0} \end{pmatrix}. \quad (22)$$

Equation (22) has been written with all the known quantities on the right-hand side. Solution of this set yields the potential distribution in the semiconductor domain, including the interface $\partial\Omega_{BC}$, and the nodal flux on $\partial\Omega_{BC}$. An integral equation similar to Eq. (B4) of the appendix can then be used to evaluate the potential at any desired location in the interior of the dielectric. Note that the system of equations given in (19) is much smaller than the finite element set, (18). Therefore, the final set, Eq. (22), is not much larger than Eq. (18). This allows us to obtain the potential in the whole domain, semiconductor and dielectric, with a numerical effort not much larger than for the semiconductor domain alone.

III. EXAMPLE

In order to demonstrate the utility of our algorithm, we now present a numerical example. We utilize the generic heterostructure shown in Fig. 2. In the semiconductor domain, a quantum wire is realized at the $\text{Al}_{0.3}\text{Ga}_{0.7}\text{As}/\text{GaAs}$ heterojunction and is defined by applying a sufficiently negative gate voltage V_g to the metal gates on the top surface. The exposed semiconductor surface resides between the gate electrodes. The n -type doping density is assumed to be 10^{18} cm^{-3} in the $\text{Al}_{0.3}\text{Ga}_{0.7}\text{As}$ layer and 10^{15} cm^{-3} in the GaAs substrate. At equilibrium the exposed semiconductor surface must support a surface charge of equal density but opposite sign to the charge density in the semiconductor, as dictated by charge neutrality. The implied value of the interface charge density Q_{int} is equal to $4.456 \times 10^{13} \text{ e}/\text{cm}^2$ for a 0.8 eV pinning en-

ergy. For simplicity, when a bias is applied, Q_{int} is assumed to be fixed at this value although this is not a limitation of the algorithm.

In this example, a typical width of 200 nm is assumed for the exposed semiconductor surface, $\partial\Omega_{CB}$. Both Schottky contacts, $\partial\Omega_{AB}$ and $\partial\Omega_{CD}$, extend laterally 700 nm from the exposed surface which is sufficient to ensure that the solution is laterally invariant at the domain boundary, that is $\partial u/\partial n = 0$. We assume a typical thickness of 40 nm for the n -type AlGaAs layer and a thickness of 1600 nm of the lightly doped GaAs substrate. The thicknesses of the GaAs layer and of the 256- μm -thick dielectric layer are chosen such that the potential far from the heterointerface and the exposed semiconductor surface is invariant at the domain boundary.

For the boundary condition at the Schottky contact, Fermi-level pinning is assumed with a typical pinning energy of 0.8 eV.^{3,7,11} The conduction band discontinuity across the heterointerface is modeled by an additional linear constraint boundary condition, $u|_1 - u|_2 = \Delta u$, and is implemented by a penalty element method.^{13,18} All simulations are performed for room temperature.

Within a semiclassical Thomas-Fermi charge model,¹⁶⁻¹⁸ the equilibrium electron and hole densities in the semiconductor domain are given by the Fermi-Dirac integral of order 1/2,

$$n(u) = N_C F_{1/2}(-u), \quad (23)$$

$$p(u) = N_V F_{1/2}\left(u - \frac{E_G}{kT}\right), \quad (24)$$

where E_G is the energy band gap, and N_C and N_V are the effective conduction and valence band density of states, respectively. As specified in Sec. II, the variable $u = [E_C(\phi) - E_F]/kT$ measures the separation of the potential-dependent conduction band edge from the Fermi level in units of kT . The densities of ionized donors and ionized acceptors are given by

$$N_D^+ = N_D / \left[1 + 2 \exp\left(-u + \frac{E_D}{kT}\right) \right], \quad (25)$$

$$N_A^- = N_A / \left[1 + 2 \exp\left(u + \frac{E_A - E_G}{kT}\right) \right], \quad (26)$$

where N_D and N_A are the doping densities of donors and acceptors, respectively, and E_D and E_A are the ionization energies for donors and acceptors, respectively. Poisson's equation can then be written as

$$\epsilon \nabla^2 u = -\frac{e^2}{kT} (p - n + N_D^+ - N_A^-). \quad (27)$$

The material parameters used herein are similar to those used by Sadao Adachi in his review paper.¹⁹

A. Numerical procedure

It is a challenging numerical problem to solve the above two-dimensional nonlinear Poisson equation for quantum structures which include heterojunctions and open boundaries. The requirements include a highly non-

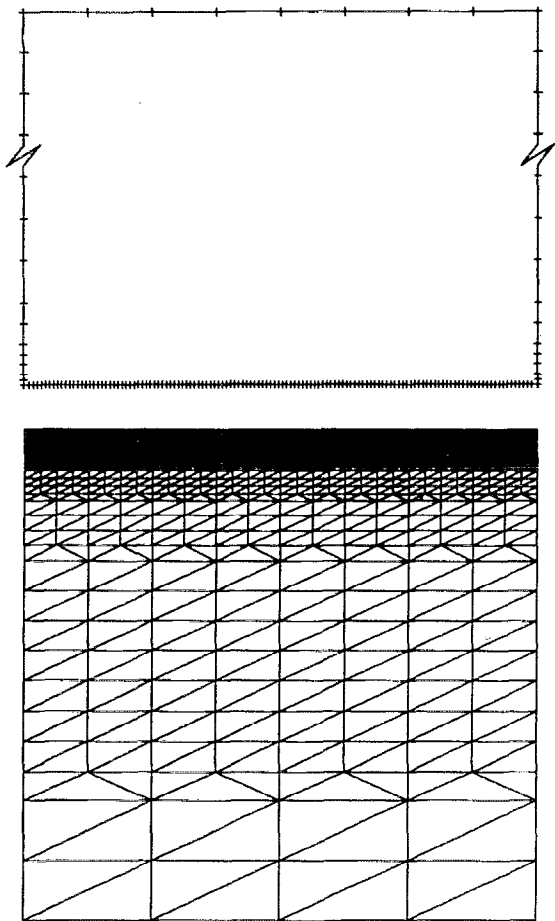


FIG. 3. Mesh used in the numerical example; upper panel shows non-uniform boundary element mesh for the dielectric region and lower panel nonuniform finite element mesh for the semiconductor domain.

uniform mesh design, both bandwidth optimization and sparse matrix techniques, and iterative linearization, each of which will be discussed in the following subsections.

1. Nonuniform FBEM mesh design

The finite element portion of the domain is discretized with two-dimensional triangular master elements. Close to the semiconductor heterointerface, the potential is expected to exhibit large variations on a nanometer length scale whereas it is expected to vary rather slowly in the semi-insulating bulk region. In order to match this nonuniform potential variation and to keep the computational size reasonably small, a highly nonuniform mesh is designed as shown in the bottom panel of Fig. 3. This mesh consists of 13 972 triangular elements and 7360 nodes. The area ratio between the largest element and the smallest element is 5120.5, where the area of the smallest element is 781.25 \AA^2 which describes the highest resolution near the heterointerface. Special four-node penalty elements are added along the heterointerface to impose the conduction band discontinuity.

The nonuniform boundary element mesh for the dielectric portion of the domain consists of 181 constant elements and is shown in the top panel of Fig. 3. Because of

the radiation property of the fundamental solution, the boundary element mesh is designed with a very large side length of $256 \mu\text{m}$, which truncates the infinite dielectric domain into the finite domain without losing required accuracy. The coupling nodes, which share both the FEM domain and the BEM domain, are designed for connecting the FEM domain with the BEM domain. Notice that in the example mesh shown in Fig. 3, the BEM domain boundary farthest from the semiconductor surface has been closed with only eight large boundary elements (shown as the eight segments of the top horizontal boundary in Fig. 3).

2. Bandwidth optimization

If we use the mesh generated by a standard mesh generator directly for the FEM procedure, the resultant system of equations, $\mathbf{K}^s \mathbf{u}^s = \mathbf{p}^s$, has a randomly populated stiffness matrix \mathbf{K}^s with a size of (7360×7360) . The distribution of nonzero elements in this matrix, results in a large bandwidth, which makes it expensive to solve this system of equations. In order to gain both storage and computational efficiency, we employ sparse matrix techniques. First, we use standard bandwidth optimization algorithms to efficiently reorder the node numbers of our FEM mesh to reduce the bandwidth between coupled equations. Then, a skyline storage scheme is used to efficiently store this sparse matrix. The final matrix represents a savings of $\sim 95\%$ of the original storage space.

3. Solution of the nonlinear system of equations

The coupled system of Eqs. (22) is nonlinear because p_f^s is a nonlinear function of the potential within the semiclassical Thomas-Fermi charge model. This nonlinear coupled system is linearized by the Continuous Newton Iteration method.²⁰ The resultant linear system of equations is solved by standard Gaussian elimination with row pivoting. The Fermi-Dirac integrals of orders $\pm 1/2$ used in the charge model are approximated by the Rational Chebyshev Polynomial with a relative error of 10^{-9} .²¹ Bandwidth optimization of the stiffness matrix in conjunction with the skyline storage technique provides an efficient solution of the linear system of equations. The Continuous Newton Iteration converges with an iterative error of 10^{-8} within 20 iterations, with a typical cumulative CPU time of 660 s on an IBM RISC System/6000.

B. Numerical results

The results shown in this section concentrate on demonstrating the utility of the FBEM algorithm, and on comparing it to other choices of boundary conditions at the exposed surface. Figure 4 shows clearly the formation of the quantum wire as a function of the gate bias. In Fig. 4(a), the conduction band edge is plotted parallel to the AlGaAs/GaAs heterointerface (on the GaAs side) for different bias conditions. Electron accumulation occurs in those regions where the conduction band dips below the semiclassical electron quasi Fermi level, which is chosen as the zero of the energy axis and indicated by the dashed line. Figures 4(b) and 4(c) show plots of the conduction

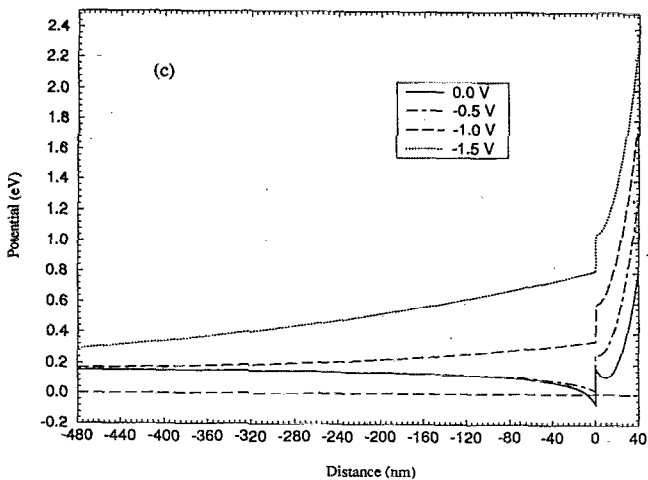
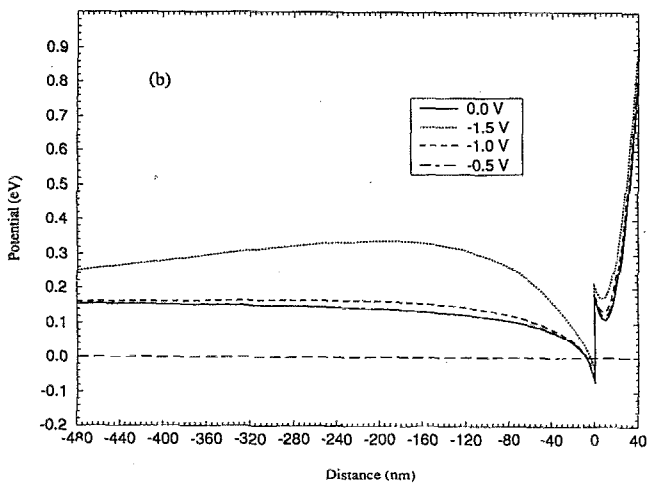
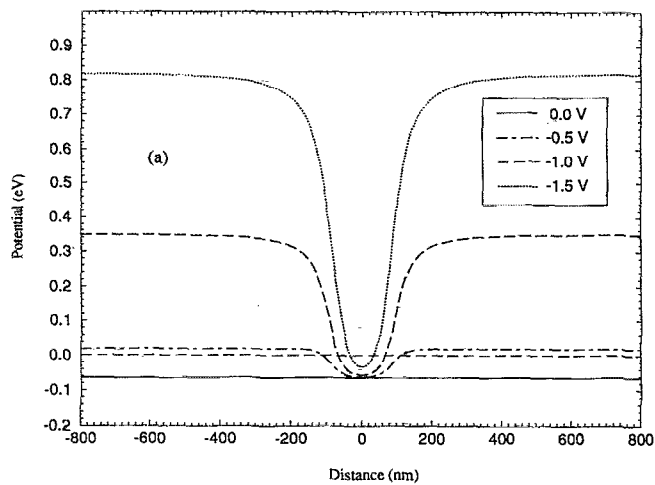


FIG. 4. Result of the FBEM algorithm showing the conduction band profiles for different bias conditions; (a) parallel to the heterointerface (on the GaAs side), (b) perpendicular to the semiconductor surface at $x=0.0$ nm (under the exposed surface), (c) perpendicular to the semiconductor surface at $x=400.0$ nm (under the biased gate.)

band profile perpendicular to the semiconductor surface at $x=0.0$ nm (under the exposed surface) and at $x=400.0$ nm (under the biased gates), respectively. We see the formation of the quantum wire for negative gate biases in

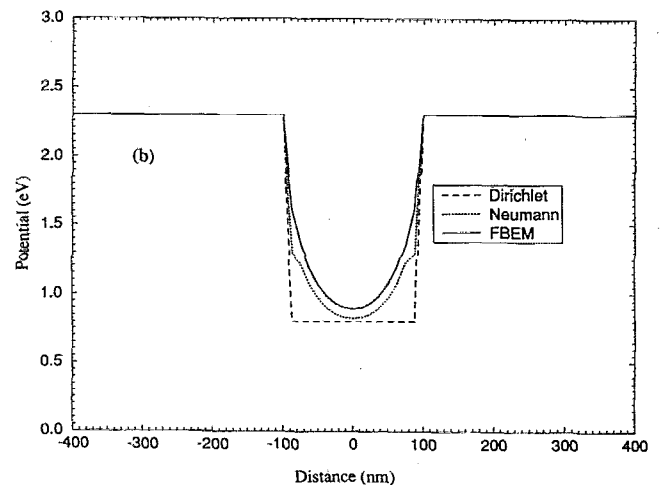
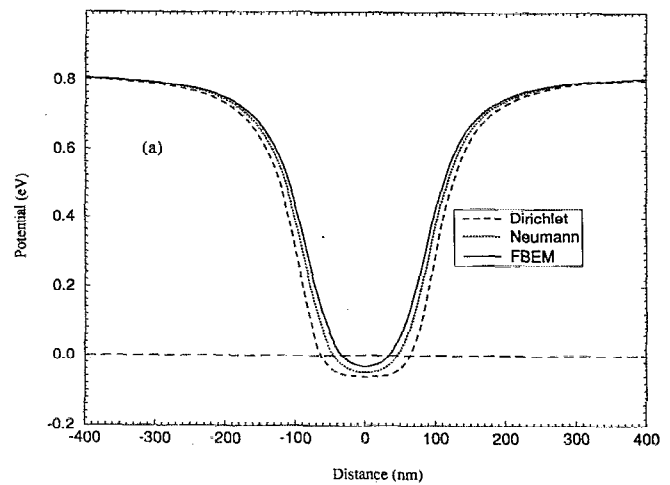


FIG. 5. Comparison of the conduction-band profiles under -1.5 V gate bias for the three types of boundary conditions on the exposed semiconductor surface; (a) parallel to the heterointerface (on the GaAs side) and (b) parallel to the semiconductor surface.

excess of -0.5 V due to the depletion of the two-dimensional electron gas underneath the metallic gates, but not underneath the exposed semiconductor surface. Possible device applications of such structures are based on the demonstrated ability to utilize the gate bias to modulate both the width of the channel and the electron density in the wire.

Figure 5 presents, for a negative gate bias of -1.5 V, a comparison of the results obtained with our FBEM algorithm and those utilizing the conventional Dirichlet or Neumann boundary conditions at the exposed semiconductor surface. For the Dirichlet boundary conditions at the exposed surface, the conduction band is assumed to be pinned at the value of 0.8 eV, regardless of gate bias. For the Neumann boundary conditions at the exposed surface, the electric field is assumed to be fixed at the exposed surface, at a value equal to the field for zero gate bias. Figure 5(a) shows this comparison for a plot of the conduction band profile parallel to the AlGaAs/GaAs heterointerface (on the GaAs side). We see that the different methods produce significantly different results. Specifi-

cally, the expected width of the electron channel differs by a factor of 2 for the Dirichlet and FBEM boundary conditions. The Dirichlet boundary conditions also predict a significantly higher electron density than the FBEM algorithm. Figure 5(b) shows the same comparison at the semiconductor surface. The center region in this figure corresponds to the exposed surface, and the split gates are shown by the fixed potential on either side. For the Dirichlet boundary conditions at the exposed surface, there is an unrealistic discontinuous step in the conduction band edge at the metallic gate. The Neumann boundary conditions also exhibit a discontinuous behavior, as opposed to the physically more appealing smooth result of the FBEM algorithm.

Judging from Fig. 5, the Neumann boundary conditions yield better results than the Dirichlet boundary conditions. We therefore suggest the use of Neumann boundary conditions for simulations which restrict themselves to the semiconductor region, as opposed to treating the full problem domain including the dielectric.

IV. CONCLUSION

We have presented a study of the boundary conditions at exposed semiconductor surfaces, which views the boundary as the interface between the semiconductor and the dielectric. We developed an algorithm, termed FBEM, which couples the two-dimensional finite element method (FEM) in the semiconductor to the boundary element method (BEM) in the dielectric. The problem domain is composed of semiconductor regions governed by the nonlinear Poisson's equation and a dielectric region governed by Laplace's equation. The interface conditions (14) and (15) combine the two regions together by matching both the potential and the normal electric flux. The size of the resultant system of equations from the FBEM method is essentially the same as that of the conventional method in which only the semiconductor region is considered. The major advantage of the FBEM algorithm is to model the exposed semiconductor surface by imposing the more physical interface matching conditions without making artificial assumption about either the potential or the electric field at the exposed surface. We also demonstrated the feasibility and utility of the FBEM algorithm by showing results for a typical split gate structure.

In ongoing work, we study the implementation of different physical models for the interface charge Q_{int} at the exposed surface, including microscopic models for surface states. These results, based on the techniques developed in this paper, will be presented in the future.

ACKNOWLEDGMENTS

The authors wish to thank Dr. Gary H. Bernstein, Mr. Henry K. Harbury, Dr. Craig S. Lent, Mr. Mark Mueller, and Mrs. Helen Zhang for numerous helpful discussions and suggestions. This work was supported in part by AFOSR, ARPA, and ONR.

APPENDIX A: FINITE ELEMENT FORMULATION OF THE POISSON PROBLEM

1. Weak variational problem in the semiconductor domain

For the semiconductor domain Ω_s , with $\Omega_s = \Omega_1 \cup \Omega_2$, we give the symmetric weak variational problem for Poisson's equation, (7). The problem may be posed as follows:

P2. Find

$$u_s \in \bar{H}^1(\Omega_s - \partial\Omega_{EH}), \quad (A1)$$

such that

$$\int_{\Omega_s} \epsilon_s \nabla u_s \cdot \nabla \omega_s dA = \int_{\Omega_s} f_s \omega_s dA + \int_{\partial\Omega_{CB}} q_s \omega_s dS, \\ \forall \omega_s \in \bar{H}_0^1, \quad (A2)$$

where

$$\bar{H}^1 = \left\{ u_s \mid \int_{\Omega_s} \nabla u_s \cdot \nabla u_s dA < \infty, \quad u_s = u_{g1} \text{ on } \partial\Omega_{BA}, \right. \\ \left. u_s = u_{g2} \text{ on } \partial\Omega_{DC}, \quad [[u_s]] = \Delta u \text{ on } \partial\Omega_{EH} \right\}, \quad (A3)$$

and

$$\bar{H}_0^1 = \left\{ \omega_s \mid \int_{\Omega_s} \nabla \omega_s \cdot \nabla \omega_s dA < \infty, \right. \\ \left. \omega_s = 0 \text{ on } \partial\Omega_{BA}, \text{ and } \partial\Omega_{DC} \right\}. \quad (A4)$$

In **P2**,

$$u_s = \begin{cases} u_1 & \text{in } \Omega_1 \\ u_2 & \text{in } \Omega_2 \end{cases} \quad (A5)$$

and

$$\epsilon_s = \begin{cases} \epsilon_1 & \text{in } \Omega_1 \\ \epsilon_2 & \text{in } \Omega_2 \end{cases}. \quad (A6)$$

2. FEM discretization

The domain Ω_s is discretized with a two-dimensional mesh with M nodal points at locations $\mathbf{x}_1, \mathbf{x}_2, \dots, \mathbf{x}_M$. We assume an approximate expression for the potential trial function $u_s(\mathbf{x})$ in terms of standard finite element shape functions¹³ as follows:

$$u_s(\mathbf{x}) = \phi(\mathbf{x}) \cdot \mathbf{u}_0^s + \phi_{BC}(\mathbf{x}) \cdot \mathbf{u}_{BC}^s, \quad (A7)$$

where the set of all nodal potentials has been partitioned into the vector \mathbf{u}_{BC}^s containing the potentials at the nodes on the interface $\partial\Omega_{BC}$ between the semiconductor and the dielectric, and \mathbf{u}_0^s contains the values of the potential at all other nodes in the semiconductor domain. The test function $\omega_s(\mathbf{x})$ is interpolated similarly,

$$\omega_s(\mathbf{x}) = \phi(\mathbf{x}) \cdot \omega_0^s + \phi_{BC}(\mathbf{x}) \cdot \omega_{BC}^s. \quad (A8)$$

We then express the gradients as

$$\nabla u_s(\mathbf{x}) = \mathbf{B}(\mathbf{x}) \cdot \mathbf{u}_0^s + \mathbf{B}_{BC}(\mathbf{x}) \cdot \mathbf{u}_{BC}^s, \quad (A9)$$

$$\nabla \omega_s(\mathbf{x}) = \mathbf{B}(\mathbf{x}) \cdot \omega_0^s + \mathbf{B}_{BC}(\mathbf{x}) \cdot \omega_{BC}^s, \quad (\text{A10})$$

The finite element approximation to Eq. (A2) can then be written as

$$\begin{aligned} \omega_0^{sT} \left\{ \int_{\Omega_s} \epsilon_s \mathbf{B}^T \mathbf{B} dA \mathbf{u}_0^s + \int_{\Omega_s} \epsilon_s \mathbf{B}^T \mathbf{B}_{BC} dA \mathbf{u}_{BC}^s \right\} \\ + \omega_{BC}^{sT} \left\{ \int_{\Omega_s} \epsilon_s \mathbf{B}_{BC}^T \mathbf{B} dA \mathbf{u}_0^s + \int_{\Omega_s} \epsilon_s \mathbf{B}_{BC}^T \mathbf{B}_{BC} dA \mathbf{u}_{BC}^s \right\} \\ = \omega_0^{sT} \int_{\Omega_s} \phi^T \mathbf{f}_s dA + \omega_{BC}^{sT} \int_{\partial\Omega_{BC}} \phi_{BC}^T \mathbf{q}_s dS. \end{aligned} \quad (\text{A11})$$

Equation (A11) must hold for all ω_0^s and ω_{BC}^s . This implies the following coupled sets of equations:

$$\begin{aligned} \left(\int_{\Omega_s} \epsilon_s \mathbf{B}^T \mathbf{B} dA \right) \mathbf{u}_0^s + \left(\int_{\Omega_s} \epsilon_s \mathbf{B}^T \mathbf{B}_{BC} dA \right) \mathbf{u}_{BC}^s \\ = \int_{\Omega_s} \phi^T \mathbf{f}_s dA, \end{aligned} \quad (\text{A12})$$

$$\begin{aligned} \left(\int_{\Omega_s} \epsilon_s \mathbf{B}_{BC}^T \mathbf{B} dA \right) \mathbf{u}_0^s + \left(\int_{\Omega_s} \epsilon_s \mathbf{B}_{BC}^T \mathbf{B}_{BC} dA \right) \mathbf{u}_{BC}^s \\ = \int_{\partial\Omega_{BC}} \phi_{BC}^T \mathbf{q}_s dS. \end{aligned} \quad (\text{A13})$$

Again, if \mathbf{q}_s is specified on $\partial\Omega_{BC}$, this set of equations may be solved for the nodal potentials, \mathbf{u}_0^s and \mathbf{u}_{BC}^s . For the problem as formulated herein the term involving \mathbf{q}_s couples the semiconductor domain to the dielectric. We may cast these equations in a more usable format by defining the following matrices and vectors:

$$\mathbf{K}_{11} = \int_{\Omega_s} \epsilon_s \mathbf{B}^T \mathbf{B} dA, \quad (\text{A14})$$

$$\mathbf{K}_{12} = \int_{\Omega_s} \epsilon_s \mathbf{B}^T \mathbf{B}_{BC} dA, \quad (\text{A15})$$

$$\mathbf{K}_{22} = \int_{\Omega_s} \epsilon_s \mathbf{B}_{BC}^T \mathbf{B}_{BC} dA, \quad (\text{A16})$$

$$\mathbf{p}_f^s = \int_{\Omega_s} \phi^T \mathbf{f}_s dA, \quad (\text{A17})$$

$$\mathbf{p}_{BC}^s = \int_{\partial\Omega_{BC}} \phi_{BC}^T \mathbf{q}_s dS. \quad (\text{A18})$$

Equations (A12) and (A13) then become

$$\begin{aligned} \mathbf{K}_{11} \mathbf{u}_0^s + \mathbf{K}_{12} \mathbf{u}_{BC}^s = \mathbf{p}_f^s, \\ \mathbf{K}_{12}^T \mathbf{u}_0^s + \mathbf{K}_{22} \mathbf{u}_{BC}^s = \mathbf{p}_{BC}^s. \end{aligned} \quad (\text{A19})$$

In the above formulation we have not assumed that the trial function satisfies the essential boundary conditions and the jump on the heterointerface. We impose these conditions on the final discretized equations by a penalty function method.^{13,18}

APPENDIX B: BOUNDARY ELEMENT FORMULATION OF THE LAPLACE PROBLEM

1. Boundary integral equation in the dielectric domain

The dielectric domain Ω_d is a homogeneous charge-free region. The governing equation is Laplace's equation. The boundary integral equation for Laplace's equation is¹⁴

$$\frac{1}{2} u_d(\xi) + \int_{\partial\Omega_d} u_d(\mathbf{x}) q^*(\xi, \mathbf{x}) dS = \int_{\partial\Omega_d} q_d(\mathbf{x}) u^*(\xi, \mathbf{x}) dS, \quad (\text{B1})$$

where $u^*(\xi, \mathbf{x})$ is the potential at \mathbf{x} given a unit point charge at ξ in an infinite domain. u^* is often referred to as the fundamental solution of Laplace's equation and $q^* = \epsilon \partial u^* / \partial n$ is the associated electric flux density. The integrals are in the sense of *Cauchy Principal Values*.

For an isotropic two-dimensional domain, the fundamental solution of Laplace's equation (8) is

$$u^*(\xi, \mathbf{x}) = \frac{1}{2\pi} \ln\left(\frac{1}{r}\right), \quad (\text{B2})$$

where $r = |\mathbf{x} - \xi|$ is the distance from the source point ξ to any point under consideration, \mathbf{x} .

By using the notation for the dielectric boundary as given in Fig. 3, the boundary integration problem (B1) can be posed as **P3**. *Find*

$$u_d(\mathbf{x}), \quad \mathbf{x} \in \Omega_d,$$

such that

$$\begin{aligned} \frac{1}{2} u_d + \int_{\partial\Omega_{BC}} u_d q^* dS + \int_{\partial\Omega_{DJ}} u_d q^* dS + \int_{\partial\Omega_{IA}} u_d q^* dS \\ - \int_{\partial\Omega_{AB}} q_d u^* dS - \int_{\partial\Omega_{CD}} q_d u^* dS + \int_{\partial\Omega_{JI}} u_d q^* dS \\ = - \int_{\partial\Omega_{AB}} u_{g1} q^* dS - \int_{\partial\Omega_{CD}} u_{g2} q^* dS + \int_{\partial\Omega_{BC}} q_d u^* dS. \end{aligned} \quad (\text{B3})$$

2. BEM discretization

The boundary element method requires the boundary of the dielectric, $\partial\Omega_d$, to be discretized and a functional form assumed for u and q over each resulting element. Herein we divide $\partial\Omega_d$ into N segments and assume u and q constant over each element. Equation (B1) can then be written for a given nodal point ξ_i as

$$\begin{aligned} \frac{1}{2} u_d(\xi_i) + \sum_{j=1}^N \left(\int_{\partial\Omega_{d_j}} q_d^*(\xi_i, \mathbf{x}_j) dS \right) u_d(\mathbf{x}_j) \\ = \sum_{j=1}^N \left(\int_{\partial\Omega_{d_j}} u_d^*(\xi_i, \mathbf{x}_j) dS \right) q_d(\mathbf{x}_j). \end{aligned} \quad (\text{B4})$$

Define the following matrices:

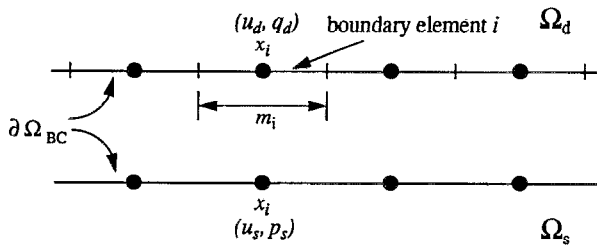


FIG. 6. A typical section of the common boundary $\partial\Omega_{BC}$ with the FEM and the BEM discretization shown separately.

$$\hat{H}_d^{ij} = \int_{\partial\Omega_{d_i}} q_d^*(\xi_i, \mathbf{x}_j) dS, \quad G_d^{ij} = \int_{\partial\Omega_{d_i}} u_d^*(\xi_i, \mathbf{x}_j) dS. \quad (B5)$$

Now let

$$H_d^{ij} = \begin{cases} \hat{H}_d^{ij} & \text{when } i \neq j \\ \hat{H}_d^{ij} + \frac{1}{2} & \text{when } i = j \end{cases} \quad (B6)$$

Then Eq. (B4) can be written as

$$\sum_{j=1}^N H_d^{ij} u_d^j = \sum_{j=1}^N G_d^{ij} q_d^j. \quad (B7)$$

This equation can also be expressed in matrix form as

$$\mathbf{H}^d \mathbf{u}^d = \mathbf{G}^d \mathbf{q}^d, \quad (B8)$$

where \mathbf{H}^d and \mathbf{G}^d are two $(N \times N)$ matrices and \mathbf{u}^d and \mathbf{q}^d are vectors of length N which contain the boundary values of the potential u and the normal flux density q .

In Appendix C, we show that by employing the interface conditions (14) and (15), the two systems of equations, (A19) and (B8), are coupled together forming a determined system of equations.

APPENDIX C: FINITE ELEMENT COUPLED WITH BOUNDARY ELEMENT FORMULATION

We define the "total flux" across a boundary segment $\partial\Omega_x$ as

$$p = \int_{\partial\Omega_x} q dS, \quad (C1)$$

where q is the normal electric flux density.

In the FEM, a total flux is associated with each node by taking a weighted average of the normal electric flux density over the elements adjacent to the node; see Eq. (A18). In the resulting FEM equations, each node has either an unknown potential u_s or an unknown total flux p_s ; see Eq. (A19). In the boundary element equations each element has an unknown potential u_d or an unknown flux density q_d . On the interface between the semiconductor and the dielectric, $\partial\Omega_{BC}$, we must impose interface Eqs. (14) and (15).

In Fig. 6, we show a typical section of the common boundary $\partial\Omega_{BC}$ with the FEM discretization and the BEM

discretization shown separately. We can impose Eq. (14) by associating the constant BEM potential for element i with node point i and write

$$u_s(\mathbf{x}_i) = u_d(\mathbf{x}_i). \quad (C2)$$

In vector form this becomes

$$\mathbf{u}_{BC}^s = \mathbf{u}_{BC}^d = \mathbf{u}_{BC}. \quad (C3)$$

The imposition of Eq. (15) is not so straightforward. As described above, the FEM has a total flux associated with node i , whereas the BEM has a constant flux density associated with element i . We convert the BEM flux density to a total flux by multiplying by the element length m_i . In matrix notation this can be written as

$$\mathbf{p}^d = \mathbf{M}^d \mathbf{q}^d, \quad (C4)$$

where \mathbf{M}^d is a diagonal matrix with entries m_i . We can then replace Eq. (15) with a total flux balance as

$$p_i^s + p_i^d = q_i \equiv \frac{e}{kT} Q_{\text{int}} m_i, \quad (C5)$$

or in vector notation

$$\mathbf{p}_{BC}^s + \mathbf{p}_{BC}^d = \mathbf{q}. \quad (C6)$$

Equation (B8) can now be converted into an "equivalent" FEM set of equations by rewriting as

$$\mathbf{M}^d \mathbf{G}^{d-1} \mathbf{H}^d \mathbf{u}^d = \mathbf{M}^d \mathbf{q}^d \equiv \mathbf{p}^d, \quad (C7)$$

or

$$\mathbf{S}^d \mathbf{u}^d = \mathbf{p}^d. \quad (C8)$$

Partitioning \mathbf{u}^d and \mathbf{p}^d similar to the finite element system of Eqs. (18), i.e.,

$$\mathbf{u}^{dT} = (\mathbf{u}_0^{dT}, \mathbf{u}_{BC}^{dT}), \quad \mathbf{p}^{dT} = (\mathbf{p}_0^{dT}, \mathbf{p}_{BC}^{dT}), \quad (C9)$$

yields Eq. (C8) in partitioned form:

$$\begin{aligned} \mathbf{S}_{11} \mathbf{u}_0^d + \mathbf{S}_{12} \mathbf{u}_{BC}^d &= \mathbf{p}_0^d, \\ \mathbf{S}_{21} \mathbf{u}_0^d + \mathbf{S}_{22} \mathbf{u}_{BC}^d &= \mathbf{p}_{BC}^d. \end{aligned} \quad (C10)$$

A new global system of equations is formed by coupling Eq. (C10) with the finite element system of Eq. (A19) and enforcing the interface conditions (C3) and (C6),

$$\begin{pmatrix} \mathbf{S}_{11} & \mathbf{S}_{12} & \mathbf{0} & \mathbf{0} \\ \mathbf{S}_{21} & \mathbf{S}_{22} & \mathbf{0} & \mathbf{I} \\ \mathbf{0} & \mathbf{K}_{12} & \mathbf{K}_{11} & \mathbf{0} \\ \mathbf{0} & \mathbf{K}_{22} & \mathbf{K}_{12}^T & -\mathbf{I} \end{pmatrix} \begin{pmatrix} \mathbf{u}_0^d \\ \mathbf{u}_{BC}^d \\ \mathbf{u}_0^s \\ \mathbf{p}_{BC}^s \end{pmatrix} = \begin{pmatrix} \mathbf{p}_0^d \\ \mathbf{q} \\ \mathbf{p}_f^s \\ \mathbf{0} \end{pmatrix}. \quad (C11)$$

¹ *Nanostructure Physics and Fabrication*, edited by M. A. Reed and W. P. Kirk (Academic, Boston, 1989).

² *Nanostructures and Mesoscopic Systems*, edited by W. P. Kirk and M. A. Reed (Academic, Boston, 1992).

³ S. Selberherr, *Analysis and Simulation of Semiconductor Devices* (Springer, Berlin, 1984).

⁴ C. S. Lent, P. D. Tougaw, W. Porod, and G. H. Bernstein, *Nanotechnology* **4**, 49 (1993); C. S. Lent, P. D. Tougaw, and W. Porod, *Appl. Phys. Lett.* **62**, 714 (1993).

⁵ S. E. Laux, NASECODE V: Proceedings of the 5th International Conference on Numerical Analysis of Semiconductor Devices and Integrated Circuits, 1987, p. 270.

⁶ A. Kumar, S. E. Laux, and F. Stern, *Phys. Rev. B* **42**, 5166 (1990).

- ⁷T. Kerkhoven, A. T. Galick, U. Ravaioli, J. H. Arends, and Y. Saad, *J. Appl. Phys.* **68**, 3461 (1990).
- ⁸U. Ravaioli, T. Kerkhoven, M. Raschke, and A. T. Galick, *Superlatt. Microstruct.* **11**, 343 (1992).
- ⁹J. H. Luscombe, A. Bouchard, and M. Luban, *Phys. Rev. B* **46**, 10262 (1992).
- ¹⁰A. Bouchard and J. Luscombe, *Nanostructures and Mesoscopic Systems*, edited by W. P. Kirk and M. A. Reed (Academic, Boston, 1992), p. 393.
- ¹¹J. H. Luscombe, *Nanotechnology* **4**, 1 (1993).
- ¹²I. Mayergoyz, *J. Appl. Phys.* **59**, 195 (1986).
- ¹³K. J. Bathe, *Finite Element Procedures in Engineering Analysis* (Prentice-Hall, Englewood Cliffs, NJ, 1982).
- ¹⁴C. A. Brebbia, J. C. F. Telles, and L. C. Wrobel, *Boundary Element Techniques* (Springer, Berlin, 1984).
- ¹⁵C. A. Brebbia and P. Georgiou, *Appl. Math. Modeling* **3**, 212 (1979).
- ¹⁶J. S. Blackmore, *Solid State Electron.* **25**, 1067 (1982).
- ¹⁷C. M. Wolfe, N. Holonyak, Jr., and G. E. Stillman, *Physical Properties of Semiconductors* (Prentice-Hall, Englewood Cliffs, NJ, 1989).
- ¹⁸W. Porod, H. K. Harbury, and S. M. Goodnick, *Appl. Phys. Lett.* **61**, 1823 (1992); H. K. Harbury, W. Porod, and S. M. Goodnick, *J. Appl. Phys.* **73**, 1509 (1993).
- ¹⁹S. Adachi, *J. Appl. Phys.* **58**, R1 (1985).
- ²⁰D. Kincaid and W. Cheney, *Numerical Analysis* (Brooks/Cole, Belmont, 1991).
- ²¹W. J. Cody and H. C. Thacher, *Math. Comput.* **21**, 30 (1967).

Journal of Applied Physics is copyrighted by the American Institute of Physics (AIP). Redistribution of journal material is subject to the AIP online journal license and/or AIP copyright. For more information, see <http://ojps.aip.org/japo/japcr/jsp>
Copyright of Journal of Applied Physics is the property of American Institute of Physics and its content may not be copied or emailed to multiple sites or posted to a listserv without the copyright holder's express written permission. However, users may print, download, or email articles for individual use.